Journal of Nuclear Materials 390–391 (2009) 900–903

Contents lists available at ScienceDirect

Journal of Nuclear Materials

journal homepage: www.elsevier.com/locate/jnucmat

Operation of ICRF antennas in a full tungsten environment in ASDEX Upgrade

Vl. Bobkov *, F. Braun, R. Dux, L. Giannone, A. Herrmann, A. Kallenbach, H.W. Müller, R. Neu, J.-M. Noterdaeme, Th. Pütterich, V. Rohde, ASDEX Upgrade Team

MPI für Plasmaphysik, Boltzmannstr. 2, D-85748 Garching, Germany

ARTICLE INFO

PACS:
52.50.G
52.40.F
52.40.H

ABSTRACT

In the 2007 and early part of 2008 experimental campaigns, ASDEX Upgrade operated with full tungsten (W) wall without boronization. Use of ICRF power results in a significant increase of W source. Low temperature conditions at the plasma facing components, achieved by a large clearance between the separatrix and the antenna (>6 cm) and by elevated gas puff rates ($> 5 \times 10^{21}$ s^{-1}) help to lower W sputtering yield during ICRF. Operation of neighboring ICRF antennas at the phase difference close to $-90°$ can lead to a reduction in the W source. However, a reduction of parallel near-fields by antenna design is needed to further minimize the W source. A relation has been established between the HFSS code calculations predicting a dominant role of box currents in the formation of parallel antenna near-fields and the experiment. The shapes of the measured vertical profile of effective sputtering yields and the calculated sheath driving voltages show a qualitative agreement. This confirms that the existing tools are a good basis to design an improved antenna.

1. Introduction

The ICRF (Ion Cylotron Range of Frequencies) system for heating and current drive is widely used in present experiments and is planned for ITER. For future devices, high-Z materials, such as tungsten (W) are candidates for the first wall [1–3]. It is therefore important to make the operation of ICRF antennas compatible with high-Z plasma facing components (PFCs). The main incompatibility issue is the enhanced erosion of PFCs connected along magnetic field lines to the active ICRF antennas [4,5]. This problem is caused by high RF electric parallel antenna near-fields $E_{\|}$ (parallel to magnetic field lines) and the corresponding high sheath driving voltages $V_{\|} = \int E_{\|} \cdot dl$ [6] along the field lines which cross the near-fields [7]. The $V_{\|}$ potentials are rectified due to the non-linearity of the plasma. The rectified voltages accelerate hydrogen ions as well as light impurity ions, such as oxygen, which sputter the high-Z PFCs.

In the 2007 and early part of 2008 experimental campaign, ASDEX Upgrade (AUG) operated with PFCs fully covered by W without boronization [8,9]. This paper discusses the operation of the ICRF antennas in the W environment and the minimization of W source during ICRF by choosing the operational parameters of AUG and ICRF system. This is followed by a discussion on the comparison of the experimental knowledge with 3D finite-element calculations of antenna near-fields.

2. ICRF antennas at ASDEX Upgrade and diagnostics

The ICRF system at AUG has 4 ICRF antennas with two straps each, placed on the low field side (LFS). The phasing of the strap currents of $(0, \pi)$ is used for standard H-minority resonance heating scheme. The antennas are equipped with 3 dB-hybrid systems [10] which isolate the RF transmitters from the antenna load. In this configuration two antennas operate simultaneously with a fixed phase of +90° between them (e.g. antennas 3 and 4 situated near each other with 1/16 sector in between, Fig. 1). The phasing is thus $(0, \pi)$,$(\pi/2, 3\pi/2)$. For a limited time during the experimental period, the 3 dB-hybrids were bypassed and antennas 3 and 4 were connected independently, each to its own RF transmitter. This was to study the influence of phase between antennas 3 and 4 on W source as well to operate these antennas in different time windows without mutual influence. Such operation was mostly limited to L-mode discharges due to the issues with antenna load tolerance without the 3 dB-configuration in H-modes. In order to study the contribution of antenna straps to $V_{\|}$, antenna 4 is equipped with W-coated shields (Fig. 1) which cover the antenna corners, where the magnetic field lines cross only one antenna strap. Antenna 4 has also a local gas puff integrated in one of the limiters, as shown in Fig. 1.

The W-coated antenna limiters of antennas 3 and 4 are monitored spectroscopically. Lines of sight (LOSs) which look on the antenna limiters are shown in Fig. 1. Eight LOSs for the antenna 3 limiter (green color in Fig. 1)[1] and five for the antenna 4 limiter

* Corresponding author.
E-mail address: Volodymyr.Bobkov@ipp.mpg.de (Vl. Bobkov).

[1] For interpretation of color in Fig. 1, the reader is referred to the web version of this article.

0022-3115/$ - see front matter © 2009 Elsevier B.V. All rights reserved.
doi:10.1016/j.jnucmat.2009.01.231

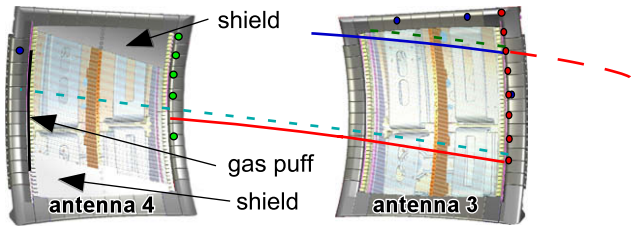

Fig. 1. Antennas 3 and 4 with points of spectroscopic observation and examples of field line connections used in Section 3.2.

(red color in Fig. 1) give information on the radial profile of tungsten and hydrogen D(H) line intensities. The intensities are linked directly to the particle fluxes (Γ_W and Γ_D correspondingly) at the points of observation [11]. Effective sputtering yields Y_W are calculated by dividing Γ_W by Γ_D measured on the same line of sight [11]. Values of Y_W are therefore independent of the absolute error of Γ measurements. For given concentrations and charge states of the light impurities (W sputtering by deuterons alone can not explain the measured sputtering yields [9]), Y_W can be translated to a rectified sheath potential drop and theoretically to RF voltage $V_{\|}$. Therefore the measured Y_W provides the link to $V_{\|}$.

The total W content during ICRF is characterized by the W concentration C_W measured spectroscopically (see, for example, [12]) for the corresponding plasma temperature in the range between 0.9 and 1.8 keV. For H-modes discharges presented in this paper this corresponds to the poloidal radius in the range from 0.4 the 0.9. For L-mode discharges the corresponding region is at poloidal radius <0.7.

3. Results and discussion

3.1. Operation of ICRF antennas with minimized tungsten sputtering yield

Application of ICRF power results in a significant (factor up to 50 higher compared to discharges without ICRF) increase of Y_W at PFCs connected to the antennas by field lines, and consequently increase in the W concentration and radiation from plasma. Several operational methods were proven successful to affect the W source during ICRF. Fig. 2 illustrates the three ways to decrease the W concentration at the plasma edge by affecting Y_W at the antenna limiters and at the PFCs during ICRF. These are: (a) increasing the separatrix-antenna clearance by reducing the outermost plasma position R_{out}; (b) increasing the gas puffing rate (works both for L- and H-modes); (c) operating the neighboring antennas 3 and 4 with a phase different from 90° which is the standard phase for the 3 dB-hybrid configuration. Data in Fig. 2(a) and (b) are taken during H-modes with neutral beam and electron cyclotron heating, while Fig. 2(c) shows the data from ICRF-only L-mode.

For the methods illustrated in Fig. 2(a) and (b), the plasma temperature at PFCs is likely an important player. At large separatrix-antenna clearance, the density at PFCs decreases while at high gas puff rate the density increases. RF near-fields are expected to increase in the first case and to decrease in the second case. Therefore it is very probable that the plasma temperature, lower in the both cases, is the crucial parameter which leads to the reduction of the W sputtering yield. Apart from the direct effect on the sheath potentials, an increase in the plasma temperature leads to an increase of the concentrations and the charge states of the background light impurities which sputter W. This plasma temperature dependence points out that an RF induced local plasma temperature increase can also contribute to W sputtering via the influence on light impurities.

The use of an additional gas puff from a local gas valve integrated in antenna 4 does not significantly change Y_W if compared to the standard midplane valves. The positive aspect of using the antenna valve is some (5–10%) relative increase of antenna 4 resistance which can be crucial for high RF power experiments. However, one has to consider that this increase is partly due to local ionization in $E_{\|}$ fields which is an additional power loss mechanism.

Fig. 2(c) shows the effect of variation of the phase between the neighboring antennas 3 and 4 in a low-density L-mode discharge. The points with the phase value of 90° correspond to the standard 3 dB-hybrid configuration. The red arrows in Fig. 2(c) show the decrease of C_W relative to the 90° phase that happens relatively fast on a background with a slowly decreasing C_W. The slow decrease is observed in many other discharges with constant phase and is

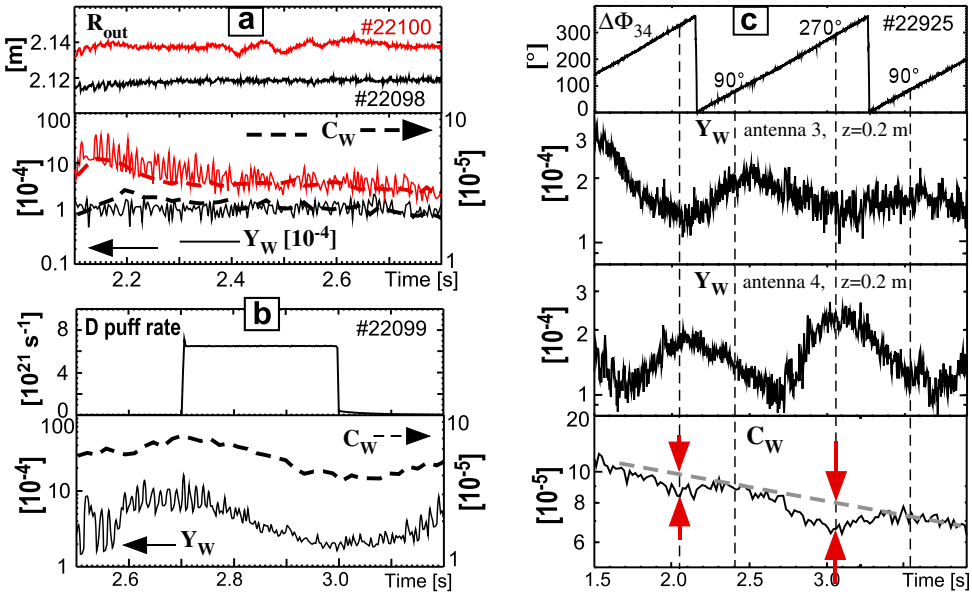

Fig. 2. Reduction Y_W and C_W during ICRF: (a) reducing the outermost plasma position (R_{out}); (b) adding gas puff; (c) changing the phase between antenna 3 and 4 from the standard +90°.

due to slowly rising density at constant deuterium puff rate. The fast decrease of C_W is due to reduction of Y_W (likely due to changes of $V_\parallel$) in many locations such as at antenna 3 with the vertical position $z = 0.2$ m (Fig. 2(c)). Broad minima in C_W are observed at the phase close to -90 (270)° at $t = 2.05$ s and $t = 3.05$ s correspondingly. Although the netto effect is the reduction of C_W, there are also locations where Y_W is increased, like $z = 0.2$ m of antenna 4 shown in Fig. 2(c). The time delay between a change in the W source (Y_W) and a corresponding change in the tungsten concentration (C_W) is small compared to the time of the phase scan. This was checked in the discharges with constant phases where the values of Y_W and C_W were found consistent with those from the dynamical phase scan. The closeness of the minima of Y_W to the phase of $-90°$ points out that either the magnetic field inclination angle is important for the double-antenna system (+90 and $-90°$ would be equal for horizontal magnetic field), or some additional mechanism is involved. It is beyond the scope of this paper to pursue the detailed interpretation of the effect of the phase difference. For a detailed study of the effect, the 3 dB-hybrid configuration should be changed to allow operation with any phase difference between the neighboring antennas. Currently, we can still state, that from the operational point of view, this effect can help to decrease the total W source.

The possibilities for the reduction of the Y_W and C_W values with existing ICRF antennas in AUG are limited in the experiment and impose by themselves limits on the operational parameters. In the case from Fig. 2(a), the clearance between the separatrix and the antenna is 8 cm for $R_{out} = 2.12$ m and it is 6 cm for $R_{out} = 2.14$ m. This leads to low antenna resistance and voltage stand-off issues in antennas and in transmission lines during the shots with higher ICRF power (>3 MW). In the case from Fig. 2(b), generally the gas puff rate of $> 5 \times 10^{21}$ s^{-1} is required and the discharges are limited to high density. In the case from Fig. 2(c), the effect on Y_W is observed for low-density discharges only.

It is therefore important to consider designing an improved antenna. For this, one needs to understand the picture of the parallel antenna near-fields in the experiment and establish a relation between the experiment and calculations. A consistency of the near-field calculations with experiment would allow to design antennas with reduced parallel near-fields using the numerical codes.

3.2. Characterization of single active antennas and calculations of near-fields

Until recently it was often considered that the parallel near-fields originate from the RF magnetic flux created directly by antenna straps. In particular, the corners of a double-strap antenna where magnetic field lines pass only one out of two $(0, \pi)$ phased straps had been considered as an important contributor to $V_\parallel$. However, this concept cannot describe some empirical findings, for example the fact that the alignment of the Faraday Screen (FS) angle with the magnetic field angle is not crucial for the impurity production by such ICRF antenna. Recent studies which include both theoretical (first with ICANT [13], then with HFSS code [15]) and experimental (Langmuir probes on Tore Supra [14]), show that all current-carrying structures surrounding the antenna, and in particular the antenna box, can produce a large contribution to $V_\parallel$. The calculations also show that the FS effectively screens $V_\parallel$ inside the antenna box, but has a little effect on the box contribution.

For the AUG antenna, calculations with 3-D finite elements HFSS code are used with a antenna planar model and a load simulated by a sea water tank placed 4 cm in front of the FS. The antenna and the water tank are placed in a cuboid with radiation conditions as boundaries. Values of $E_\parallel$ and $V_\parallel$ are calculated at the antenna plane 1 cm in front of FS (close to the surface of the antenna limiters).

The calculations reveal that the box currents have a dominant contribution to $V_\parallel$. To prove this experimentally, antenna 4 was equipped with corner shields which screen the regions where the contributions from antenna straps are not compensated. The calculations show that $V_\parallel$ have about the same values both for the covered and the uncovered antennas due to the dominant contribution of the antenna box currents. In order to assess the validity of the calculations, spectroscopic measurements are used.

Fig. 3 shows the vertical Y_W profiles on antenna 3 (uncovered) and antenna 4 (covered) in an L-mode discharge with ICRF only heating and with the large separatrix-antenna clearance. The values for each antenna are normalized to a maximum value Y_W^{max} at each antenna to compensate for the small (≈20%) difference between antennas due to a toroidal asymmetry of the in-vessel components. The experimental conditions were chosen to be as close to the vacuum conditions in simulations as possible and to reduce the sensitivity of the measurements to the distance between points of observation and plasma. The latter helps to compensate for some small misalignment between the poloidal shapes of magnetic configuration of the discharge and the antenna limiter contour. The data are taken from the time windows when first antenna 3 and then antenna 4 is operated alone, and correspond to 1 MW of power.

The spectroscopical observation points at the vertical positions $z = 0.3$ m and $z = 0.4$ m for antenna 3 and antenna 4 show about the same Y_W/Y_W^{max} values for both antennas, whereas antenna 4 has the cover at these locations. These values are also very large compared to the level of the sputtering yields in ohmic discharge which is a factor of 10 lower than the maximum value during ICRF. This observation confirms that the covers of antenna 4 do not affect $V_\parallel$ considerably. Therefore a different effect plays a more important role than the effect of uncompensated strap contributions. This effect is likely due to the box currents. This is also indicated on the $z = 0.53$ m line of sight on antenna 3, which is situated on the very outer edge of the antenna and is not connected along field lines to any antenna strap. The value of Y_W/Y_W^{max} measured here is close to 1.

For a further comparison between experiment and calculations, the restrictions apply due to the use of sea water in the HFSS calculations instead of a plasma model. The radial distribution of the rectified fields and the absolute values of the sheath potential drop can not be predicted accurately. However, a qualitative comparison of the shapes (not absolute values) of poloidal profiles of the measured Y_W and $V_\parallel$ calculated by taking integral of $E_\parallel$ according to [6] is to some extent possible, because both are linked to the sheath potential drop. As mentioned above, $V_\parallel$ is calculated at the antenna plane just in front of the limiters.

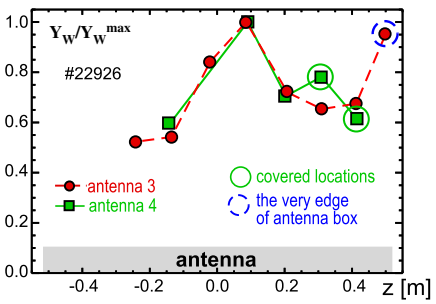

Fig. 3. Vertical Y_W profile measured on antenna 3 (red, dashed, circles) and antenna 4 (green, solid, squares) normalized to the maximum value Y_W^{max}. $P_{ICRF} = 1$ MW from one antenna only. (For interpretation of the references to colour in this figure legend, the reader is referred to the web version of this article.)

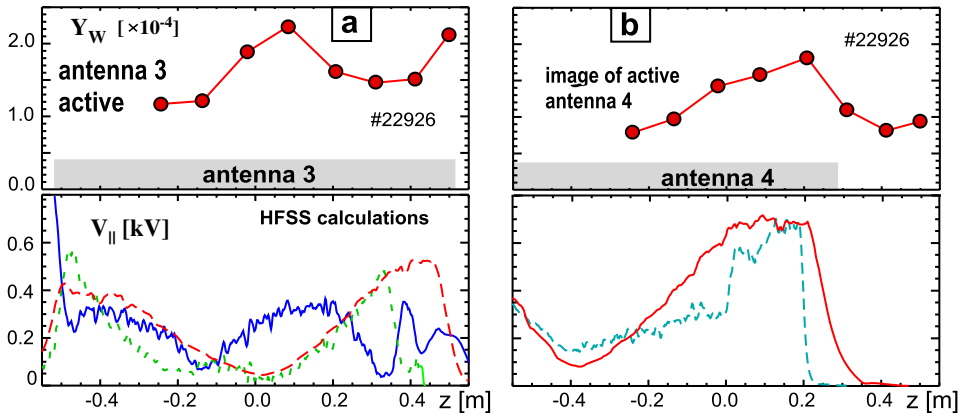

Fig. 4. (a) Upper: Y_W profile on antenna 3, only antenna 3 is on. Lower: $V_{||}$ from HFSS for different field line geometries. (b) Upper: Y_W profile on antenna 3, only antenna 4 is on. Lower: $V_{||}$ from HFSS for the two most probable line geometries.

We compare the shape of Y_W vertical profile measured when antenna 3 only is operated (upper graph in Fig. 4(a)) with the shape of $V_{||}$ profile from the HFSS code. Both experimental data and calculations correspond to the antenna power of 1 MW coupled. The voltages (curves in the lower graph in Fig. 4(a)) are calculated for the different field line geometries starting at the observation locations of antenna 3 limiter. Three main geometries can be distinguished, the examples of which are shown on the upper part of antenna 3 in Fig. 1 and correspond to the same colors and curve types in Fig. 4(a). The different field line geometries should be taken into account because the spectroscopic measurements integrate toroidally over a relatively broad emission region. An observation spot has a 3 cm diameter and covers both sides of the limiter. The experimental data in Fig. 4(a) are therefore affected by all the field line geometries. Furthermore, the relative contribution of the different geometries to the measured sputtering yield can change from one vertical location to another due to changing field line connection length and variations of the shape of limiter tiles in the regions of observation. The experimental data correspond better to the RF voltages calculated for the type of the field line geometry shown as solid blue curve. However, it is difficult to make any conclusive statement on relation between the experiment and the calculations under these conditions.

The situation becomes easier if the right limiter of antenna 3 is used to characterize antenna 4 at the time when antenna 4 only is operated (Fig. 4(b)). This limiter provides a projection following the magnetic field lines biased by antenna 4. From the previous experiments [15] we know that the Y_W values measured on the locations mapped to an active antenna can be high at large separatrix-antenna clearance. In this case we again consider the field lines starting from the antenna 3 limiter. For the magnetic configuration used, only two main field line geometries should be considered. Examples of the field lines are illustrated in Fig. 1 (lines starting on the lower part of antenna 3). The voltages calculated along the field lines of these geometries and mapped on the vertical axis z have similar profiles (lower graph of Fig. 4(b)), and the relative differences of field line connection lengths are not as large as in the case of Fig. 4(a). Another advantage here is that the limiter area observed spectroscopically covers the whole limiter area affected by antenna 4. The shapes of measured vertical Y_W profile and $V_{||}$ from the calculations in Fig. 4(b) show qualitatively similar behaviour. It is worth to note that Y_W measured on the field lines passing above antenna 4 are higher than those in ohmic discharges. A non-zero $V_{||}$ can be present on these field lines due to a contribution from the in-vessel structures surrounding the antenna. These structures can act similarly to the antenna box and are not included in the HFSS model.

The consistency between the experiments and the calculations encourages the use of such calculations with HFSS to design antennas with reduced parallel near-fields.

4. Conclusions

With the existing antennas in AUG, three experimental ways to reduce the W sputtering yield during ICRF were found: increase separatrix-antenna clearance, increase gas puff and operate two neighboring antennas with a phase different from the standard +90°, in particular close to −90°. Especially the first two are ITER-relevant, because the large plasma-antenna gaps are expected as well as the additional gas puff, initially planned to increase the antenna resistance.

The comparison of spectroscopical measurements with the calculations by 3D-finite elements code HFSS confirms the result from the calculation that in AUG the box currents play a dominant role in forming sheath driving voltages on the magnetic field lines connected to the antennas. Furthermore, a qualitative agreement can be found between shapes of the vertical profiles of the effective sputtering yields measured and the sheath driving voltages predicted. This encourages the use of the calculations to design an antenna with reduced parallel near-fields.

References

[1] V. Phillips et al., Plasma Phys. Control. Fusion 42 (2000) B293.
[2] A. Kallenbach et al., Plasma Phys. Control. Fusion 47 (2005) B207.
[3] B. Lipschultz et al., Nucl. Fusion 41 (2001) 585.
[4] S. Wukitch et al., J. Nucl. Mater. 363–365 (2007) 491.
[5] Vl. Bobkov et al., J. Nucl. Mater. 363–365 (2007) 122.
[6] F. Perkin, Nucl. Fusion 29 (4) (1989) 583.
[7] J.-M. Noterdaeme, AIP Conference Proceedings, vol. 244, AIP Press, Melville, NY, 1992. p. 71.
[8] R. Neu, Plasma Phys. Control. Fusion 49 (12B) (2007) B59.
[9] R. Dux et al., J. Nucl. Mater. 390–391 (2009) 858.
[10] J.-M. Noterdaeme, S. Wukitch, D.A. Hartmann, M. Brambilla, F. Braun, et al., in: Proceedings of 16th International Conference on Fusion Energy, Montreal, vol. 3, 1996, p. 335.
[11] R. Dux et al., J. Nucl. Mater. 363–365 (2007) 112.
[12] R. Neu et al., Nucl. Fusion 45 (2005) 209.
[13] L. Colas, S. Heuraux, S. Brémond, G. Bosia, Nucl. Fusion 45 (2005) 767.
[14] L. Colas et al., J. Nucl. Mater. 363–365 (2007) 555.
[15] Vl. Bobkov et al., AIP Conference Proceedings, vol. 933, AIP Press, Melville, NY, 2007, p. 83.